A Topologically Driven Glass in Ring Polymers
Supplementary Information Appendix

Davide Michieletto[1] and Matthew S. Turner[2]

[1] *School of Physics and Astronomy, University of Edinburgh, Edinburgh, United Kingdom*
[2] *Department of Physics, University of Warwick, Coventry, United Kingdom*

Computational Details

We model the system by enclosing $N = 50$ semi-flexible bead-spring polymers formed by M beads in a box with periodic boundary conditions of linear size L. The monomer density $\rho = NM/L^3 = 0.1\sigma^{-3}$ is fixed and we vary the length of the polymers and the size of the box to keep the density constant. The chains are modelled via the Kremer-Grest worm-like chain model [1]. as follows: Let r_i and $d_{i,j} \equiv r_j - r_i$ be respectively the position of the center of the i-th bead and the vector of length $d_{i,j}$ between beads i and j, the connectivity of the chain is treated within the finitely extensible non-linear elastic model with potential energy,

$$U_{FENE}(i, i+1) = -\frac{k}{2} R_0^2 \ln \left[1 - \left(\frac{d_{i,i+1}}{R_0} \right)^2 \right]$$

for $d_{i,i+1} < R_0$ and $U_{FENE}(i, i+1) = \infty$, otherwise; here we choose $R_0 = 1.6\,\sigma$ and $k = 30\,\epsilon/\sigma^2$ and the thermal energy $k_B T$ is set to ϵ. The bending rigidity of the chain is captured with a standard Kratky-Porod potential,

$$U_b(i, i+1, i+2) = \frac{k_B T l_p}{2\sigma} \left[1 - \frac{d_{i,i+1} \cdot d_{i+1,i+2}}{d_{i,i+1} d_{i+1,i+2}} \right],$$

where we set the persistence length $l_p = 5\sigma$. The steric interaction between beads is taken into account by a truncated and shifted Lennard-Jones (WCA) potential

$$U_{LJ}(i, j) = 4\epsilon \left[\left(\frac{\sigma}{d_{i,j}} \right)^{12} - \left(\frac{\sigma}{d_{i,j}} \right)^6 + 1/4 \right] \theta(2^{1/6}\sigma - d_{i,j}).$$

where $\theta(x)$ is the Heaviside function.

Denoting by U the total potential energy, the dynamic of the beads forming the rings is described by the following Langevin equation:

$$m\ddot{r}_i = -\xi \dot{r}_i - \nabla U + \eta \tag{1}$$

where ξ is the friction coefficient and η is the stochastic delta-correlated noise. The variance of each Cartesian component of the noise, σ_η^2 satisfies the usual fluctuation dissipation relationship $\sigma_\eta^2 = 2\xi k_B T$.

As customary [1] we set $m/\xi = \tau_{LJ} = \tau_{Br}$, with the LJ time $\tau_{LJ} = \sigma\sqrt{m/\epsilon}$ and the Brownian time $\tau_{Br} = \sigma/D_b$, where $D_b = k_B T/\xi$ is the diffusion coefficient of a bead of size σ, is chosen as simulation time step. From the Stokes friction coefficient of spherical beads of diameters σ we have: $\xi = 3\pi\eta_{sol}\sigma$ where η_{sol} is the solution viscosity. It is possible to map this to real-time units by using the nominal water viscosity, $\eta_{sol} = 1\,cP$ and setting $T = 300$ K and σ equal, for instance, to the diameter of hydrated B-DNA ($\sigma = 2.5\,nm$), for which one has $\tau_{LJ} = \tau_{Br} = 3\pi\eta_{sol}\sigma^3/\epsilon \simeq 37\,ns$. The numerical integration of Eq. (1) is performed by using a standard velocity-Verlet algorithm with time step $\Delta t = 0.01\tau_{Br}$ and is implemented in the LAMMPS engine.

System Preparation and Equilibration

The systems are prepared by placing the rings randomly in a very large box. The linking number between all pairs of rings is also checked in order to avoid linked polymers. In addition, the rings are initialised as perfect circles in order to avoid self-knotting. The desired monomer density is achieved by slowly shrinking the box until the target box size is reached (effectively applying a constant pressure). At this stage, we checked for unwanted linked rings and found none. After this, we equilibrate the systems by performing standard runs (with no rings artificially pinned) for at least the time need for the chains to displace their centres of mass of several R_g's. We observe that $t = 10^7\tau_{Br}$ time-steps are enough to obtain this condition. After the equilibration we performed another run in order to study the free, *i.e.* unperturbed, behaviour of the system. The mean square displacement obtained from this run is reported in see Fig. S4. The simulations in which we artificially pin some of the rings are then started from the late stages of this last run, so that the initial configuration for these *perturbed* simulations were un-correlated from the initial system set up. The rings that are artificially pinned are chosen at random among the N rings. Because the simulations are very computationally expensive, we only perform one
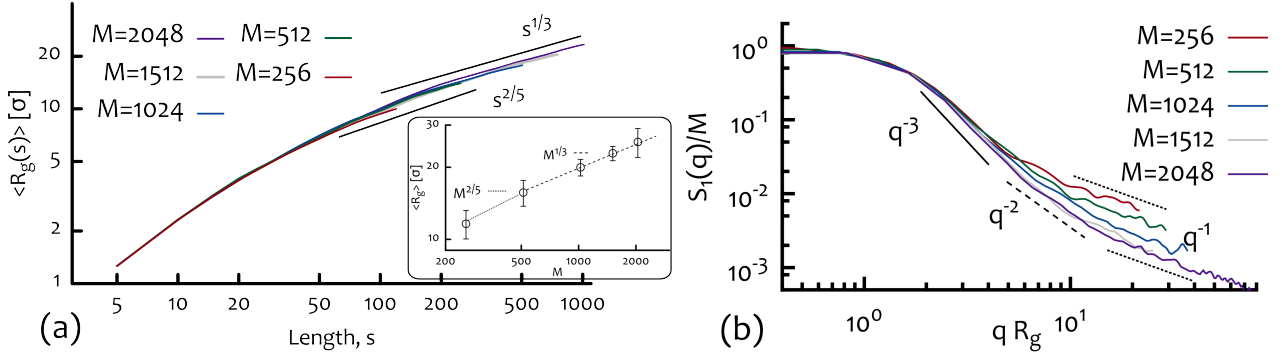
FIG. S1: (a) Ensemble average of the radius of gyration $\langle R_g \rangle \equiv \langle R_g^2 \rangle^{1/2}$ and plotted against rings' contour length s (main) and total length M (inset) both in units of the bead size. As reported in the literature, the rings show a collapsed behaviour for large M. (b) Static scattering function $S_1(q)$ plotted against qR_g and normalised by the length of the rings M. This quantity indicates a complex arrangement of the rings internal structure, which does not seem to follow a unique fractal dimension at all lengths.

simulation for each choice of c. For the longest chains reported here ($M = 2048$ beads) each run up to $2 \ 10^7 \ \tau_{Br}$ takes up to 4 weeks when running in parallel over 64 processors. This time-window has to be run for every choice of the fraction of pinned chains c. As we tested four choices of c, the results reported only for the system with $M = 2048$ (Fig. 3(e) in main text) take ~ 4 months of 64 CPUs time or, equivalently, ~ 20 years of single CPU time.

The Size and Static Structure of Rings are in Agreement with the Crumpled Globule Behaviour

In agreement with results reported in the literature [2, 3] we observe (Fig. S1) that the radius of gyration of the rings scales as $R_g \sim M^\nu$ with $\nu \simeq 1/3$ in the limit of large polymerisation index M, while we observe $\nu \simeq 2/5$ for shorter rings. This is supported by the measurement of $\langle R_g^2 \rangle$ either for the whole rings or as a function of the contour length s. The values of the exponents are in agreement with previously reported findings and we refer to previous works[2, 3] for dedicated measurements of ν. Another way of investigating the conformation of the rings is by measuring the static structure factor. For wave-vectors in the range $1/R_g < q < 1/\sigma$, one should expect that $S_1(q)$ defined as

$$S_1(q) = \left\langle \frac{1}{M} \sum_{i,j \in I}^{M} e^{i\boldsymbol{q}(\boldsymbol{r}_i(t) - \boldsymbol{r}_j(t))} \right\rangle \tag{2}$$

where the indexes i,j run over ring I, to give $S_1(q) \sim q^{-D_F}$ [4], where D_F is the fractal dimension of the chain at length scale $1/q$ and it is related to the scaling exponent ν as $D_F = 1/\nu$. Linear chains in the melt display $D_F = 2$ for a broad range of q's [1] while we observe the rings to have a more complex organisation with D_F ranging from $D_F \simeq 3$ to $D_F \simeq 1$ at large q, in agreement with previous findings [2] (see Fig. S1).

The Contact Surface of the Coils Grows Extensively with the Length of the Rings

In order to quantify the degree of interaction between coils, we investigate (i) the number of surface monomers, (ii) the number of contiguous chains and (iii) the number of neighbouring chains.

(i) The number of surface monomers m_s is computed by counting the number of beads forming the chains that are in contact with beads forming any other chains, according to the contact matrix in eq. 3 of the main text, *i.e.* any two beads are in contact if their position is closer than $d = \rho^{-1/3}$, where $1/\rho = 10\sigma^3$ is the free volume per bead.

(ii) The number of contiguous chains n_c is computed the number of chains that have surface beads that are in contact.

(iii) The number of neighbouring chains n_n is instead defined as the number of coils that are closer than $2Rg$ to any one other coil.

These quantities are reported in Fig. S2.

The surface monomers show a near extensive dependence to the length of the rings, as already observed in previous works [2], while the number of contiguous and neighbouring chains show a similar scaling behaviour as a function of M, although n_c is found systematically larger than n_n. This may imply large fluctuations in the rings conformations, which bring distant coils in contact.
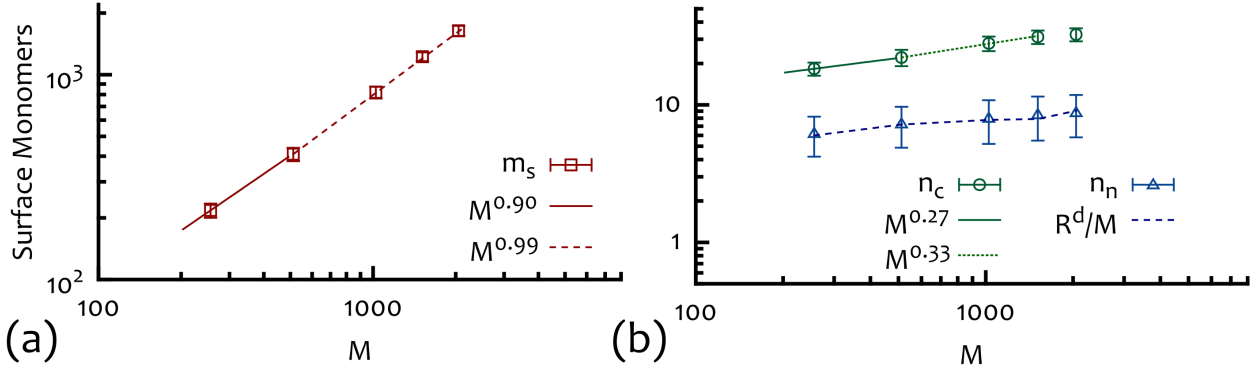
FIG. S2: (a) The number of surface monomers m_s shows a scaling $m_s \sim M^{\beta_c}$ with $\beta_c \simeq 0.99$ for the longest chains. (b) The number of contiguous chains n_c and number of neighbouring chains n_n is shown. While their scaling behaviour is similar, the average number of chains in contact at any time is systematically larger than the number of chains whose centre of mass is closer than $2R_g$. This may imply large fluctuations in the rings conformations that bring distant chains in contact with one another. In (b) we show two curves with exponents 0.33 and 0.27 as a guide for the eye but refer to the literature and further studies for more precise estimates.

The Contact Probability Shows a Decay Consistent with the Mean-Field Estimate $\gamma = 1$

The contact probability is defined as

$$P_c(|i-j|) = \left\langle \frac{1}{M} \sum_{i=1}^{M-1} \sum_{j=i+1}^{M} \Theta(a - |\boldsymbol{r}_i(t) - \boldsymbol{r}_j(t)|) \right\rangle \tag{3}$$

where $\Theta(x)$ is the Heaviside function and a is the chosen cut-off. In Fig. S3 we report P_c for two value of a and for different chain lengths. The behaviour of $P_c(m)$ is expected to follow the crumpled globule scaling

$$P_c(m) \sim m^{-\gamma} \tag{4}$$

with $\gamma \gtrsim 1$, and for which the mean field value $\gamma = \nu d$ is a lower bound. We here observe $\gamma \simeq 1.02 - 1.09$ (see Fig. S3). The prediction that fixes the sum of the contact exponent γ and the surface exponent β_c equal to 2 in the case of crumpled globules ($\nu = 1/3$), i.e. $\beta_c + \gamma = 2$ [5], is therefore here recovered within errors.

The Pair Correlation Function Suggest that the Coils are Largely Inter-Penetrating

In order to probe the inter-penetration of the coils one can also investigate the pair correlation function $g(r)$ which we here defined similarly to a recent work [6]

$$g(r) = \frac{2}{N(N-1)} \sum_{I=1}^{N-1} \sum_{J=N+1}^{N} \delta[|\boldsymbol{r}_{CM,I}(t) - \boldsymbol{r}_{CM,J}(t)| - r] \tag{5}$$

where $\boldsymbol{r}_{CM,I}$ indicates the position of the centre of mass of ring I.

This function has been used in a recent work [6] probing the glassy dynamics of polymers under confinement and we here find well characterising the degree of overlap between coils. The behaviour of $g(r)$ (reported in Fig. S3) in fact shows a distinct peak at $r_c \simeq 1.8R_g$ for $M = 256$ and at $r_c \simeq 1.4R_g$ for $M \geq 512$. This implies that the coils, although crumpled, are strongly overlapping.

The Mean Squared Displacement of the Unperturbed System is in Agreement with Previous Observations

In Fig. S4 we report the rings centre of mass mean square displacement $g_3(t)$ defined as

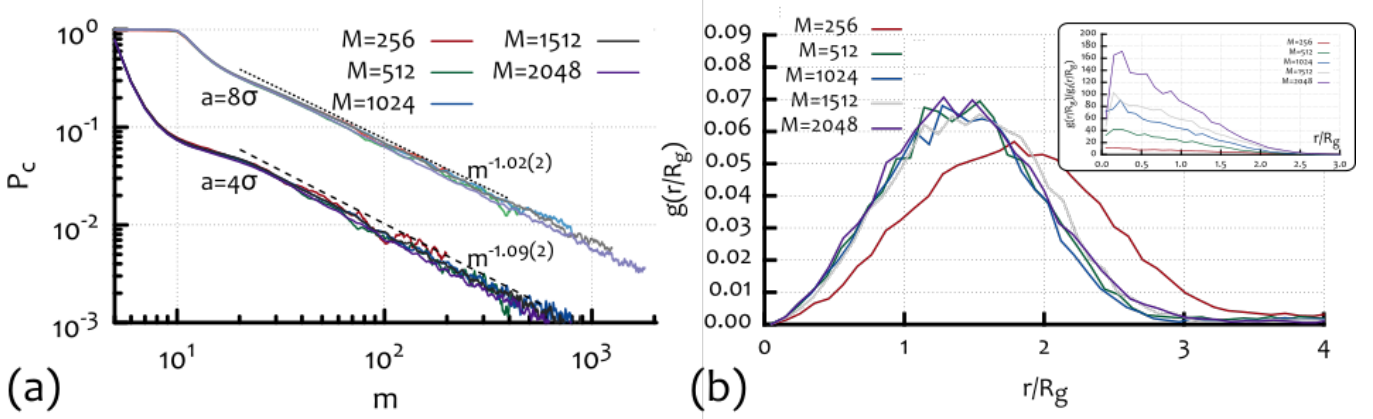$$g_3(t) = \left\langle [\boldsymbol{r}_{CM}(t) - \boldsymbol{r}_{CM}(0)]^2 \right\rangle, \tag{6}$$

FIG. S3: (a) The contact probability function $P_c(m)$ (defined in eq. (3)) shows a scaling behaviour $m^{-\gamma}$ with γ slightly dependent on the choice of the cut-off a but compatible with previous findings [2]. (b) Pair correlation function $g(r)$ for the rings centre of mass as defined in eq. (5). The peak position imply that the coils are largely overlapping. In the inset we report $g(r)$ normalised by the ideal pair distribution function $g_I(r) = 4\pi\rho_c r^2$, where $\rho_c \equiv N/L^3$ is the coils' density. The coils behave as ultra-soft sphere with large inter-penetrations.

along with the diffusion coefficient $D_{CM} \equiv \lim_{t\to\infty} g_3(t)/6t$ and the relaxation time τ_R defined via the following condition

$$g_3(\tau_R) \equiv R_g^2. \tag{7}$$

As one can notice, the mean square displacement (MSD) of the centre of mass displays an intermediate sub-diffusive regime in which $g_3(t) \sim t^{3/4}$ before crossing over to a diffusive regime at large times. This is most evident for longer rings. The scaling of the diffusion coefficient as a function of the rings length is comparable to the one found in Ref. [3] although slightly smaller, which is in agreement with the lower monomer density considered in this work. This scales asymptotically as

$$D_{CM} \sim M^{-2} \tag{8}$$

as well as the relaxation time τ_R for which we find

$$\tau_R \sim M^{2.3}. \tag{9}$$

Persistent Contiguous Chains show an Exponentially Slow Uncorrelation Time

In the main text we report the behaviour of the correlation function $\varphi_{\rm nc}(t)$, characterising the exchange dynamics of the coils. In Fig. S5 we report the values of the relaxation time of the exchange dynamics $\tau_{\rm nc}$ and the value of the stretching exponent β_{nc} used to fit the data to stretched exponentials of the form

$$\varphi_{\rm nc} = \exp\left[-\left(\frac{t}{\tau_{nc}}\right)^{\beta_{nc}}\right]. \tag{10}$$

We also report the value of $T_{\rm nc}$, which is here defined as

$$T_{\rm nc} \equiv \int_0^\infty \varphi_{\rm nc}(t)dt. \tag{11}$$

Both relaxation times τ_{nc} and $T_{\rm nc}$ are observed to grow exponentially in M. The stretching parameter β_{nc} is found to reach values close to $1/2$ for the longest chains studied in this work. This implies that the exchange time of the rings becomes extremely slow in the limit of large M and in turn this may suggest the onset of a glassy dynamics (see discussion of Fig. 2 in the main text).

The Overlap Parameter Shows an Arrested Decay Corresponding to Caged Length-Scales

The overlap parameters $Q_s^{\rm mon}(t)$ and $Q_s^{\rm coil}(t)$ are useful to characterise the glassy dynamics [7]. We here define them here as follows:

$$Q^{\rm mon}(t;c) = \langle\Theta(w - |r_i(t) - r_i(0)|)\rangle \tag{12}$$
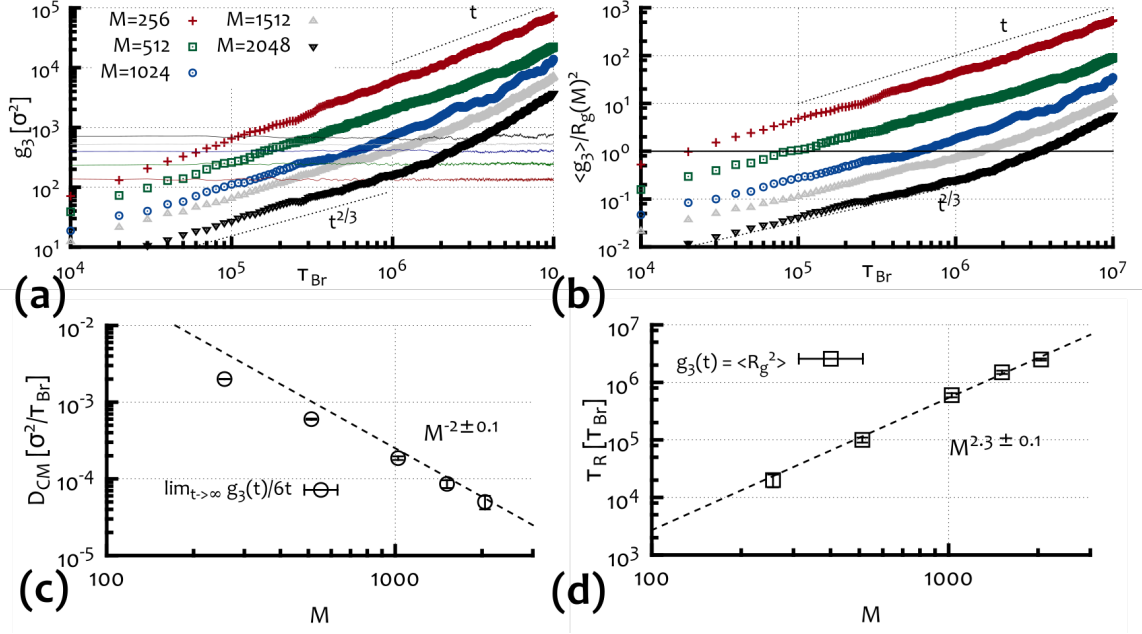
FIG. S4: (a) $g_3(t)$: Mean square displacement (MSD) of the rings centre of mass. The faint horizontal lines represent the square radius of gyration $\langle R_g^2(t) \rangle$. (b) $g_3(t)/R_g^2$: MSD of the rings centre of mass divided by their squared gyration radius. The solid horizontal line in (b) marks the value $g_3(t)/R_g^2 = 1$ at which the rings have, on average, travelled once their own size. (c) and (d) Report the behaviour of the diffusion coefficient of the centre of mass of the rings and the relaxation time τ_R (see eq. (7)), respectively. By fitting the last three data-points in order to obtain the asymptotic values of D_{CM} for large M we obtain -2 ± 0.1. By considering all data point we obtain a value for the exponent of D_{CM} of around 1.8 ± 0.1.
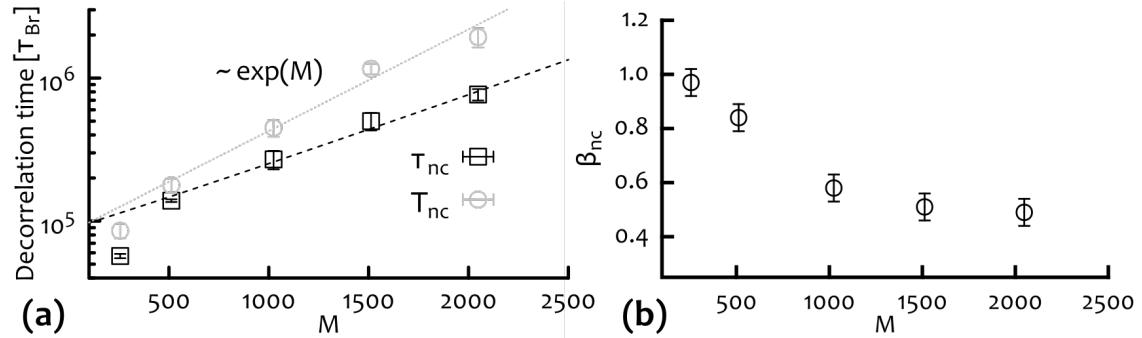

FIG. S5: (a) Values of the relaxation times τ_{nc} and T_{nc} for the contiguous correlation function $\varphi_{nc}(t)$ reported in Fig. 2 of the main text. We observe an exponential increase of the typical exchange time for large M. (b) Value of the stretching exponent β_{nc}, ranging from near unity for $M = 256$ to around $1/2$ for $M = 2048$.

and

$$Q^{\text{coil}}(t; c) = \langle \Theta(w - |\boldsymbol{r}_{CM}(t) - \boldsymbol{r}_{CM}(0)|) \rangle. \tag{13}$$

Where the average is performed over monomers (coils) and initial times. The window parameter is chosen to be $w = 2R_g$ being the length-scale at which the glassy dynamics is conjectured to occur. In other words, we aim to average out all the jiggling of the coils inside cages of size $2R_g$ and to capture the slowing down of the translational dynamics of the centre of mass of the coils. As shown in Fig. S6, this two-point correlation function clearly reflects the arrested relaxation when c is increased toward $c^\dagger$. As discussed in the main text, coils that are completely caged cannot escape and freely diffuse. This means that their centre of mass is confined in a cage of linear size $2R_g$ at all times. The coils' overlap parameter reflects the constraint by arresting its decay and in particular we find that

$$\lim_{t \to \infty} Q^{\text{coil}}(t; c^\dagger) \simeq 1 \tag{14}$$

at any time.

One can also notice that the dynamics of the beads is less constrained than the dynamics of the centre of mass of the coils when $c \to c^\dagger$. As observed, at $c \simeq 0$ one notices that the two correlation functions match in the limit of large t. On the contrary, at $c > 0$, their
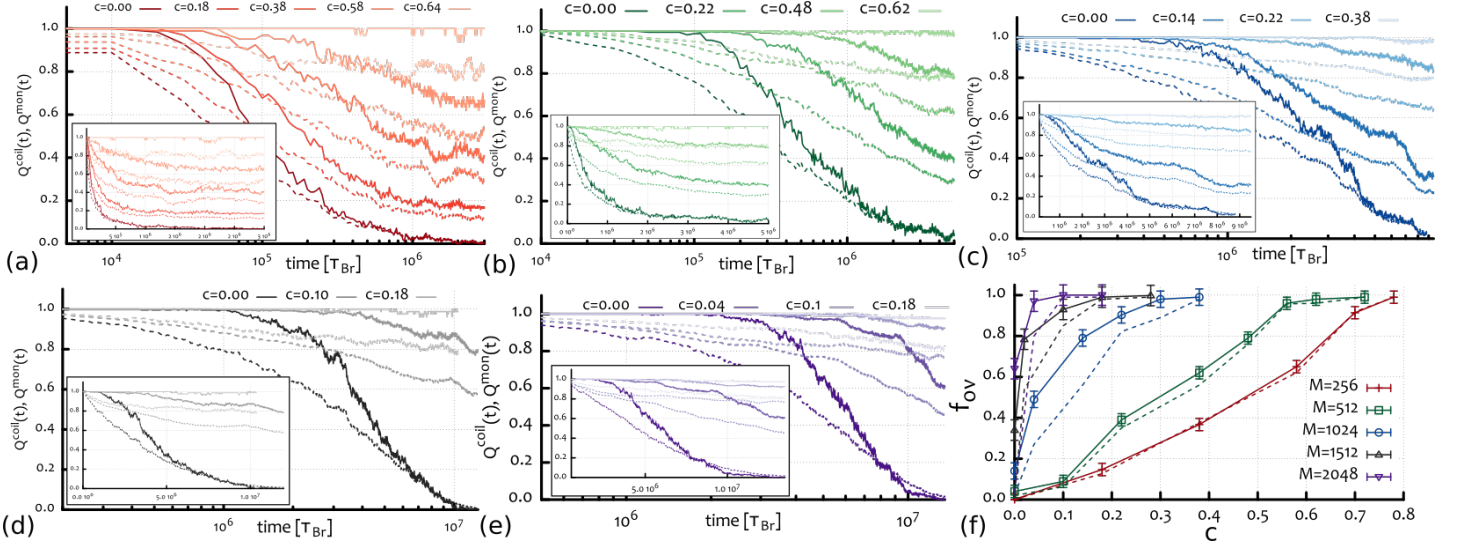
FIG. S6: Overlap parameters Q^{coil} (solid lines) and Q^{mon} (dashed lines) for different values of c and for the 5 values of M considered: (a)$M = 256$, (b)$M = 512$, (c)$M = 1024$, (d)$M = 1512$ and (e)$M = 2048$. In the inset the overlap parameter is plotted in linear scale to highlight the long time flattening. (f) The value of the overlap parameter $f_{ov} \equiv Q^{coil}(t = t_i; c)$ is evaluated and reported at two arbitrary (long) times $t_1 = 5\ 10^6\ \tau_{Br}$ (solid lines and data points) and $t_2 = 10^7\ \tau_{Br}$ (dashed lines), showing a consistent increased tendency to display an arrest of the decay at larger values.
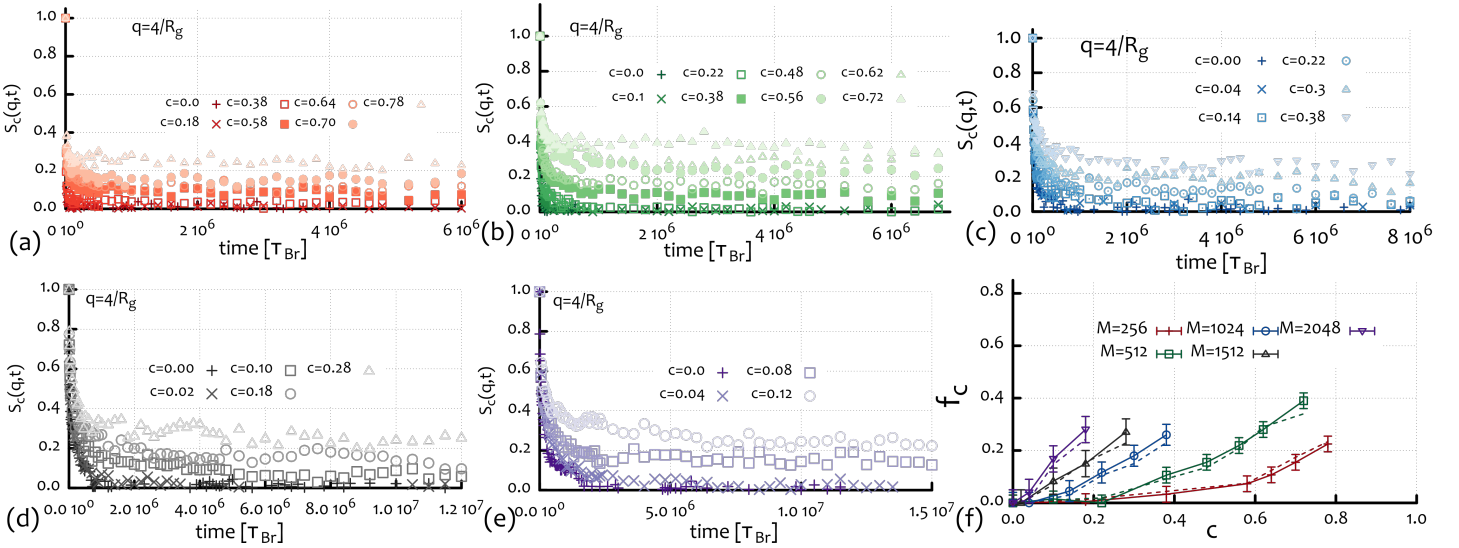

FIG. S7: Scattering function $S_c(q, t)$ computed at $q = 4/R_g$ for different chain lengths: (a)$M = 256$, (b)$M = 512$, (c)$M = 1024$, (d)$M = 1512$ and (e)$M = 2048$. The last three set of curves are plotted in linear scale to highlight the behaviour at large times. (f) The value of the scattering function at arbitrary time $\bar{t}$, $f_c \equiv S_c(q, \bar{t})$ is plotted against c for two chosen values of time $\bar{t}$: $t = 5\ 10^6\ \tau_{Br}$ (solid lines and symbols), $t = 10^7\ \tau_B r$ (dashed lines) and for the different chain lengths.

difference remains finite at all times and this implies that the relaxation dynamics is decoupled by the topological constraints, which suppress the degree of freedom of the centre of mass of the coils while leaving shorter segments along the chains relatively unhindered.

Given the fact that the arrested decay of $Q^{coil}(t; c)$ and $Q^{mon}(t; c)$ ends with an unambiguous flattening at a constant value at long times only for small chains, we compare the behaviour of this correlation function by choosing two arbitrary (long) times (t_1 and t_2) and plotting the value of $f_{ov} \equiv Q^{coil}(t = t_i; c)$ at those times in Fig. 6(f). One can clearly notice that by increasing c any system becomes slower and for larger chains, a small contamination of frozen chains (c) is enough to dramatically arrest the decay of the overlap function.
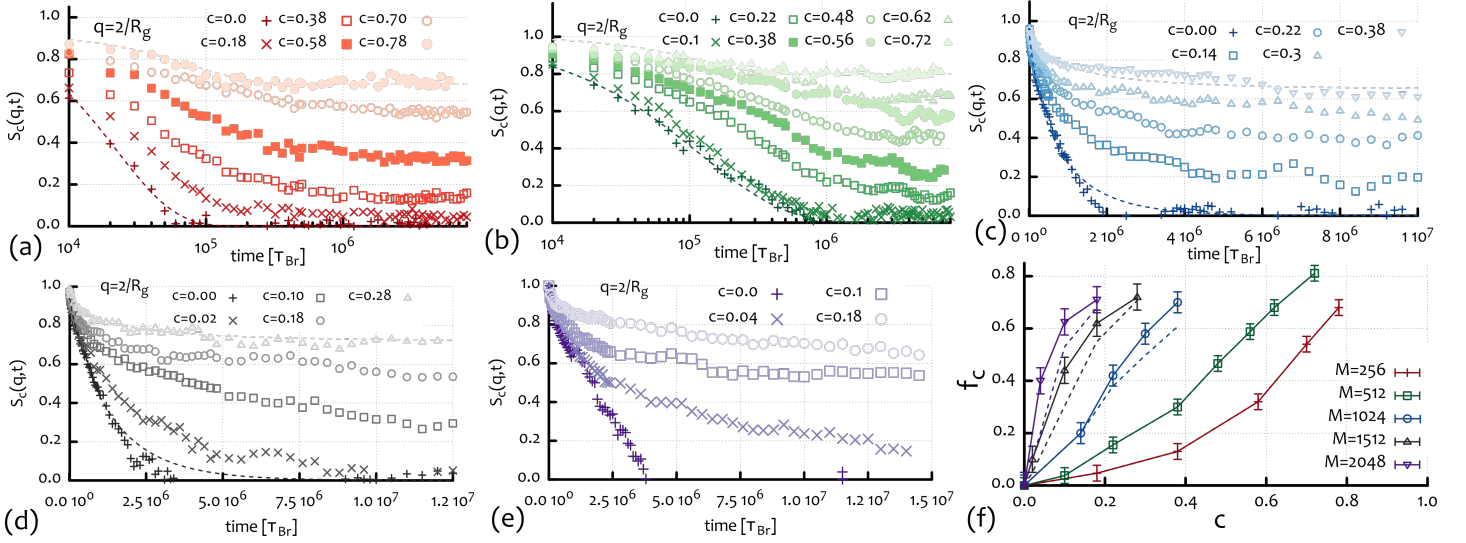
FIG. S8: Scattering function $S_c(q,t)$ computed at $q = 2/R_g$ for different chain lengths: (a)$M = 256$, (b)$M = 512$, (c)$M = 1024$, (d)$M = 1512$ and (e)$M = 2048$. The last three set of curves are plotted in linear scale to highlight the behaviour at large times. **(f)** The value of the scattering function at arbitrary time $\bar{t}$, $f_c \equiv S_c(q,\bar{t})$ is plotted against c for two chosen values of time $\bar{t}$: $t_1 = 5 \ 10^6 \ \tau_{Br}$ (solid lines and symbols), $t_2 = 10^7$ τ_{Br} (dashed lines) and for the different chain lengths.

The Scattering Function Indicates Markedly Different Relaxation Times Above and Below the Average Size of a Coil

In this section we discuss the dynamic scattering function

$$S_c(q,t) = \left\langle \frac{1}{M} \sum_{i,j \in I}^{M} e^{i\boldsymbol{q}[\boldsymbol{r}_i(0) - \boldsymbol{r}_j(t)]} \right\rangle, \tag{15}$$

calculated for $q_1 = 4/R_g$ and $q_2 = 2/R_g$. The latter explores length scales larger than the diameter of the coils ($l_2 = \pi R_g > 2R_g$) twice as long of the former, which probes length scales shorter than the diameter of the coils ($l_1 = (\pi/2)R_g < 2R_g$). As one can notice from Fig. S7 and Fig. S8, these two dynamics are markedly different.

It is clear from Figs. S7 and S8 that length scales larger than $2R_g$ are much slower than the internal modes, probed by $S_c(q = 4/R_g, t)$. This is shows by the large-time value attained by $S_c(q,t)$, defined as f_c, in the two cases and reported in S7(f) and S8(f). In the figures, we show f_c computed for two arbitrarily long times (solid and dashed lines), as done for the overlap function. The way in which f_c grows steeper and steeper for $q = 2/R_g$ and for increasing chain lengths as a function of c is indicative that the pinning procedure affects large length scales more severely than shorter ones.

From these findings, as discussed in the main text, we argue that the relaxation of the long wave length modes is strongly hindered by the pinned rings, while the short wavelength are relatively free to relax. This once again implies that the stronger effect of the pinning of rings is experienced by the translational degrees of freedom of the rings while it leaves short segments of the rings able to partially re-arrange their conformations.

The Efficiency of Freezing Grows Exponentially with the Chains' Length

The freezing procedure described in the main text offers a pathway to generate glassy states by exploiting the topology of the constituents. We show how the fraction of freely diffusing chains depends on the fraction of (non-)frozen chains in Fig. S9(a). This is done by tracking the individual MSD of the coils centre of mass and by counting the number of these which have travelled more than $2R_g$ at the end of the simulation run time and by classifying these as freely diffusing. The dashed line represents the curve followed by the data points if every non-explicitly frozen chain were free to diffuse. The deviation from this (zero pinning efficiency) line becomes stronger as the chains become longer and readily show that long chain are very sensitive to a small amount of explicitly frozen chains.

Fig. S9(b) shows the number of caged chains as a function of rings' length. Once again we identify the caged coils by tracking the individual MSD of the centre of mass and by identifying as "caged" those which have not travelled more than $2R_g$ at the end of
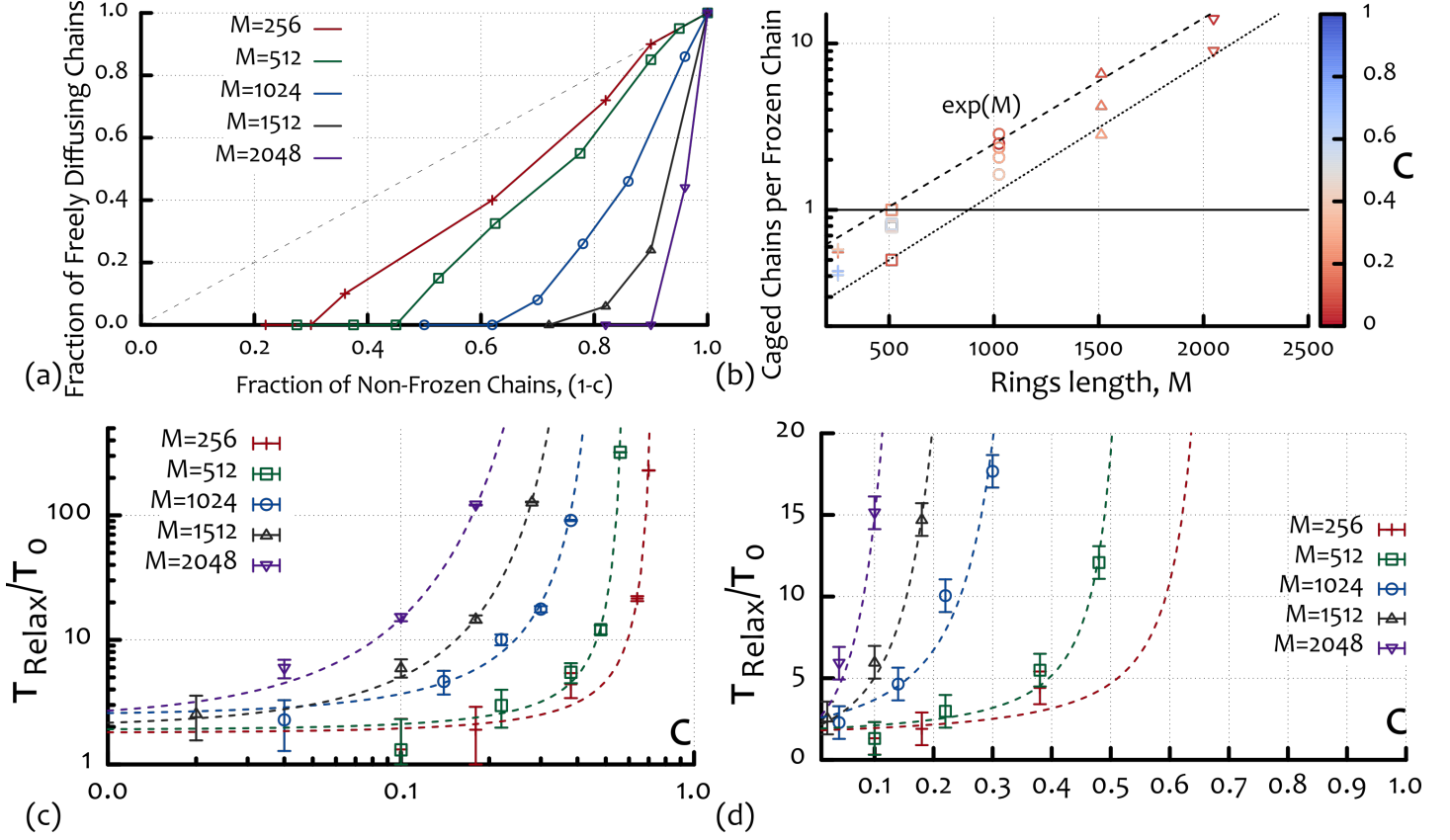
FIG. S9: **(a)** Fraction of freely diffusing rings $\Phi_{fd} = n_{fd}/(1-c)N$ against the fraction of non-frozen chains $1-c$. The dotted line marks the case in which all the non explicitly frozen chains are also freely diffusing. **(b)** The "efficiency" of the pinning procedure can be quantified by plotting the number of caged rings per frozen chain as a function of the chains' length and for the various c used. Here the points plotted mark the result from a simulation for fixed c and M. Both the most and the least efficient cases (for a given rings length M) show an exponential growth with M. **(c)-(d)** Relaxation time of the systems computed as R_g^2/D_{eff}. The divergence of the relaxation as a function of the freezing fraction c is broadly captured by a VFT function, *i.e.* $\tau_{\text{Relax}} = \tau_0 \exp[Ac/(c_0-c)]$, where c_0 is generally larger than $c^\dagger$ defined using D_{eff} (see main text).

the simulation. We repeat this analysis for every choice of c. We observe that not all simulations have the same caging "efficiency" but, remarkably, we observe that both the least and the most efficient (highest and lowest number of caged rings per frozen one) scale exponentially with M. This finding strongly encourages further computational and experimental studies of this system, as the number of chains implicitly caged can become arbitrarily big depending on the choice of M. Because of this exponential increase, fewer explicitly frozen chains will be needed to significantly slow down the system, raising the possibility that the system might spontaneously vitrify.

Finally, we study the longest relaxation time of the perturbed systems by computing $\tau_{\text{Relax}} \equiv R_g^2/D_{\text{eff}}$ and we report the findings in Figs. S9(c)-(d). The divergence of the relaxation time follows naturally from the fact that D_{eff} is vanishing at $c \to c^\dagger$. In addition, we fitted the values of τ_{Relax} with an empirical function inspired to the standard Vogel-Fulcher-Tammann function used to describe the relaxation of glass-forming systems

$$\tau_{\text{Relax}} = \tau_0 \exp\left[\frac{Dc_0}{c_0-c}\right]. \tag{16}$$

where here c replaces T. This result can be understood in terms of cooperativity of the chains: as one gets closer to the critical line $c^\dagger(M)$, the activation energy to re-arrange and relax the system becomes higher, as the number of topological constraints becomes closer to the critical value for which all the translational degrees of freedom of the system are quenched. On the other hand, it is important to notice that we can track the relaxation time of the chains only up to roughly two orders of magnitude larger than the unperturbed relaxation time (τ_0) and this is far too small a range to draw definite conclusions on the nature of this divergence.

[1] Kremer K, Grest GS (1990) Dynamics of entangled linear polymer melts: A molecular-dynamics simulation. J Chem Phys 92(8):5057.

[2] Halverson JD, Lee WB, Grest GS, Grosberg AY, Kremer K (2011) Molecular dynamics simulation study of nonconcatenated ring polymers in a melt. I. Statics. J Chem Phys 134(20):204904.

[3] Halverson JD, Lee WB, Grest GS, Grosberg AY, Kremer K (2011) Molecular dynamics simulation study of nonconcatenated ring polymers in a melt. II. Dynamics. J Chem Phys 134(20):204905.

[4] de Gennes PG (1979) Scaling concepts in polymer physics (Cornell University Press).

[5] Halverson JD, Smrek J, Kremer K, Grosberg A (2014) From a melt of rings to chromosome territories: the role of topological constraints in genome folding. Rep Prog Phys 77:022601.

[6] Kang H, Yoon Y, Thirumalai D, Hyeon C (2015) Confinement-Induced Glassy Dynamics in a Model for Chromosome Organization. Phys. Rev. Lett. 115, 198102.

[7] Karmakar S, Parisi G (2013) Random pinning glass model. Proc Natl Acad Sci USA 110(8):1-6.